Young's modulus of single-walled nanotubes

A. Krishnan
NEC Research Institute, Inc., 4 Independence Way, Princeton, New Jersey 08540-6685

E. Dujardin
Laboratoire de Chimie des Interactions Moléculaires, Collège de France, 75005 Paris, France

T. W. Ebbesen
NEC Research Institute, Inc., 4 Independence Way, Princeton, New Jersey 08540-6685
and ISIS Louis Pasteur University, 67000 Strasbourg, France

P. N. Yianilos and M. M. J. Treacy
NEC Research Institute, Inc., 4 Independence Way, Princeton, New Jersey 08540-6685
(Received 14 May 1998)

We estimate the stiffness of single-walled carbon nanotubes by observing their freestanding room-temperature vibrations in a transmission electron microscope. The nanotube dimensions and vibration amplitude are measured from electron micrographs, and it is assumed that the vibration modes are driven stochastically and are those of a clamped cantilever. Micrographs of 27 nanotubes in the diameter range 1.0–1.5 nm were measured to yield an average Young's modulus of $\langle Y\rangle = 1.25$ TPa. This value is consistent with previous measurements for multiwalled nanotubes, and is higher than the currently accepted value of the in-plane modulus of graphite. [S0163-1829(98)00144-1]

I. INTRODUCTION

Carbon fibers are widely used to reinforce other materials because of their mechanical properties and their low density.[1] It is known that the strength of the fibers increases with graphitization along the fiber axis. Therefore, carbon nanotubes, which are formed of seamless cylindrical graphene layers, represent the ideal carbon fiber and should presumably exhibit the best mechanical properties. This feature is probably the most promising for applications of nanotubes given the importance of extremely strong light-weight composites. Theoretical calculations have predicted a wide range of Young's moduli Y for very small single shell nanotubes [0.5–5.5 TPa (Refs. 2–4)].[1–9] The reference point in these studies is the Y of graphite for which the best experimental estimate is 1.02 TPa.[5] The earliest experimental measurement of Young's modulus of multishell nanotubes gave a value 1.8 ± 0.9 TPa obtained by measuring thermal vibrations using transmission electron microscopy (TEM).[6] Later, a slightly smaller value of 1.3 TPa was obtained by atomic force microscopy.[7] The measurement of single-shell nanotubes is even more difficult due to their small diameters ($\sim$1.4 nm) and because they tend to form bundles.

Here we have applied the technique of Treacy *et al.*[6] to measure Young's modulus of many isolated single-shell tubes. We also describe a least-squares optimization procedure for extracting accurately the nanotube dimensions and vibration amplitude directly from digital images. This procedure assumes only that the vibration profile is that of a clamped cantilever. We find an average value of $\langle Y\rangle = 1.25 -0.35/+0.45$ TPa, which is consistent with the results for multishell tubes. We discuss the implications of this result in terms of earlier work and the accepted Y value of graphite.

II. STOCHASTICALLY DRIVEN OSCILLATOR

The relationship between Young's modulus Y, length L, inner and outer tube radii b and a, and the standard deviation σ of the vibration amplitude at the tip of a nanotube at temperature T was presented without derivation in a previous report.[6] For completeness we present the derivation here.

In the limit of small amplitudes, it is well known that the motion of a vibrating rod is governed by the fourth-order wave equation

$$\frac{\partial^2 y}{\partial t^2}+\frac{YI}{\rho A}\frac{\partial^4 y}{\partial x^4}=0 \tag{1}$$

which has solutions of the type

$$y=\cos(c\alpha^2 t)[B\cos\alpha x+C\sin\alpha x +D\cosh\alpha x+E\sinh\alpha x] \tag{2}$$

with

$$c^2=\frac{YI}{\rho A}. \tag{3}$$

α is the wave number, Y is Young's modulus, I is the second moment of the cross-sectional area A, and ρ is the density of the rod material. For a clamped cantilever of length L, the boundary conditions are

$$y_{x=0}=0;\quad \left.\frac{\partial y}{\partial x}\right|_{x=0}=0;\quad \left.\frac{\partial^2 y}{\partial x^2}\right|_{x=L}=0;\quad \left.\frac{\partial^3 y}{\partial x^3}\right|_{x=L}=0; \tag{4}$$

yielding the solution for the nth harmonic

 ©1998 The American Physical Society

$$y_n(x,t)=\frac{u_n}{2}\cos(c\alpha_n^2 t)\left[\cos\alpha_n x-\cosh\alpha_n x+\frac{\sin\alpha_n L-\sinh\alpha_n L}{\cos\alpha_n L+\cosh\alpha_n L}(\sin\alpha_n x-\sinh\alpha_n x)\right]. \tag{5}$$

u_n is the amplitude of the nth harmonic at the tip, $x=L$. The constraints on possible values of α_n are

$$\cos\alpha_n L\cosh\alpha_n L=-1. \tag{6}$$

The total energy E_n contained in the vibration mode n can be found either by calculating the kinetic energy at the instant that $\cos(c\alpha_n^2 t)=0$, when the deflection is everywhere zero, or by calculating the elastic energy at the instant of maximum deflection when the cantilever is momentarily stationary, $\cos(c\alpha_n^2 t)=1$,

$$E_n^{\text{kinetic}}=\left[\frac{\rho A}{2}\int_0^L\left(\frac{\partial y_n}{\partial t}\right)^2 dx\right]_{t=\pi/c\alpha_n^2},$$
$$E_n^{\text{elastic}}=\left[\frac{YI}{2}\int_0^L\left(\frac{\partial^2 y_n}{\partial x^2}\right)^2 dx\right]_{t=0}, \tag{7}$$

which, after substitution for $y_n(x,t)$ from Eq. (5) and integration, both give

$$E_n=\frac{YILu_n^2\alpha_n^4}{8}. \tag{8}$$

The kinetic energy integral ignores the small angular momentum component that comes from the slight rotational motion of the rod about the fixed end, and the elastic energy integral assumes that the local radius of curvature R is given by $1/R=\partial^2 y/\partial x^2$. Both of these assumptions are valid in the limit of small deflections.

For a cylindrical rod of length L and outer and inner radii a and b, respectively, the second moment of area is $I=\pi(a^4-b^4)/4$. For convenience, we substitute

$$\beta_n=\alpha_n L \tag{9}$$

to get

$$E_n=\frac{\pi\beta_n^4}{32}\left[\frac{Y(a^4-b^4)}{L^3}\right]u_n^2. \tag{10}$$

For simplicity, we rewrite Eq. (10) in the form

$$E_n=\frac{1}{2}c_n u_n^2, \tag{11}$$

where the effective spring constant for mode n is $c_n=\pi\beta_n^4 Y(a^4-b^4)/16L^3$.

The values of β_n are the solutions to the equation $\cos\beta_n\cosh\beta_n=-1$. $\beta_0\approx 1.875\,104\,07$ for the fundamental mode, and $\beta_1\approx 4.694\,091\,13$, $\beta_2\approx 7.854\,757\,44$, $\beta_3\approx 10.995\,540\,73$, and $\beta_4\approx 14.137\,168\,39$ for the first four overtones. As n increases, $\beta_n\approx(n+1/2)\pi$.

For the next step, we need to calculate the form of the vibration profile of the tip. For a classical simple harmonic oscillator of amplitude u_n, the oscillator position y at time t is given by

$$y=u_n\sin(\omega t), \tag{12}$$

where, as before, u_n is the amplitude which depends on the energy of the oscillator, and $\omega=2\pi/f$, with f being the frequency. In the interval y to $y+dy$, the oscillator spends a time dt, which is found by taking the derivative of Eq. (12),

$$dy=u_n\omega\cos(\omega t)dt \tag{13}$$

or

$$dt=\frac{dy}{\omega\sqrt{u_n^2-y^2}};\quad -u_n\leqslant y\leqslant u_n. \tag{14}$$

The probability $P(u_n,y)dy$ of finding the oscillator between y and $y+dy$ when the amplitude is u_n is proportional to the time spent in this interval, dt. After normalization, we find

$$P(u_n,y)=\begin{cases}1/\pi\sqrt{u_n^2-y^2}, & |y|\leqslant u_n\\ 0, & |y|>u_n.\end{cases} \tag{15}$$

$P(u_n,y)$ is peaked at the extrema, $y=\pm u_n$, and has a minimum at $y=0$. However, the energy of the system, and hence the amplitude u_n, is changing in a stochastic manner with time. Therefore, we need also to average over all the possible values of u_n that the system can adopt. Further, we must also average over all of the activated modes.

Nanotube vibrations are essentially elastically relaxed phonons which are in equilibrium with the ambient at temperature T. The probability that the system is in the state m of energy $E_n=m\hbar\omega_n$ is given by the Boltzmann factor

$$W(m)=\frac{\exp(-m\hbar\omega_n/kT)}{\sum_{p=0}^{\infty}\exp(-p\hbar\omega_n/kT)}=\exp(-m\hbar\omega_n/kT)[1-\exp(-\hbar\omega_n/kT)]. \tag{16}$$

The frequency ω_n of mode n of a vibrating nanotube of density ρ is given by

$$\omega_n=2\pi f_n=\frac{\beta_n^2}{2L^2}\sqrt{\frac{Y(a^2+b^2)}{\rho}}. \tag{17}$$

The energy in mode n is therefore quantized in units of $\hbar\omega_n$. For typical nanotubes, we estimate that ω_0 is typically in the 1 MHz–10 GHz range, thus typically $\hbar\omega_n/kT\ll 1$ for the first 1000 or so modes. Thus, to a very good approximation

$$W(m)\approx\frac{\hbar\omega_n}{kT}\exp(-m\hbar\omega_n/kT). \tag{18}$$

If we set $E_n=m\hbar\omega_n$ and $dE_n\equiv\hbar\omega_n$, then in the continuum limit we get the probability $W(E_n)dE_n$, that at any instant there is between E_n and E_n+dE_n of energy in the mode n, to be

$$W(E_n)dE_n \approx \frac{1}{kT}\exp(-E_n/kT)dE_n. \quad (19)$$

This result is expected when the thermal average number of phonons, $kT/\hbar\omega_n$, is high. The average energy is $\langle E_n\rangle = kT$, half of which comes from the kinetic energy degree of freedom, and the other half from the elastic energy degree of freedom.

The stochastically averaged probability amplitude is therefore

$$\langle P(y)\rangle = \int_0^\infty P(u_n, y)W(E_n)dE_n, \quad (20)$$

which from Eqs. (15) and (19) is

$$\langle P(y)\rangle = \frac{1}{\pi kT}\int_0^\infty \frac{\exp(-E_n/kT)}{\sqrt{u_n^2 - y^2}}dE_n; \quad y^2 \le u_n^2. \quad (21)$$

From Eq. (8),

$$u_n^2 = 2E_n/c_n = \frac{32}{\pi\beta_n^4}\frac{L^3}{Y(a^4-b^4)}E_n, \quad (22)$$

therefore

$$\langle P(y)\rangle = \frac{1}{\pi kT}\int_{c_n y^2/2}^\infty \frac{\exp(-E_n/kT)}{\sqrt{2E_n/c_n - y^2}}dE_n. \quad (23)$$

The substitution

$$E_n = c_n y^2(1+x^2)/2; \quad dE_n = c_n y^2 x dx \quad (24)$$

ensures that the condition $E_n \ge c_n y^2/2$ is met. Thus,

$$\langle P(y)\rangle = \frac{c_n}{\pi kT}\exp(-c_n y^2/2kT)\int_0^\infty x\exp(-c_n y^2 x^2/2kT)dx. \quad (25)$$

The integral is easily worked out to give the Gaussian form

$$\langle P(y)\rangle = \sqrt{\frac{c_n}{2\pi kT}}\exp\left(-\frac{c_n y^2}{2kT}\right). \quad (26)$$

Using Eq. (22), the standard deviation is

$$\sigma_n^2 = \frac{kT}{c_n} = \frac{16}{\pi\beta_n^4}\frac{L^3 kT}{Y(a^4-b^4)}. \quad (27)$$

Since all the modes are independent, their contributions add incoherently. To average incoherently over all the modes n, we simply add the variances σ_n^2 to get another Gaussian distribution with a resultant standard deviation given by

$$\sigma^2 = \sum_{n=0}^\infty \sigma_n^2 = \frac{L^3 kT}{Y(a^4-b^4)}\frac{16}{\pi}\sum_{n=0}^\infty \beta_n^{-4} = 0.4243\frac{L^3 kT}{Y(a^4-b^4)}. \quad (28)$$

The constant is dominated by the $n=0$ fundamental mode, which contributes 97% of its value.

This result is equivalent to that stated in Eq. (22) for a single mode oscillation, except that we have replaced u_n with the rms amplitude σ and set $E = kT/2$ for the average elastic energy in each mode.

Remarkably, the resultant rms vibration profile along the length of the nanotube is found to be closely similar to that for a cantilever that is displaced by a lateral force $F = kT/\sigma$ applied at the tip. The rms displacement u_x as a function of position x is given accurately by the simple form

$$u_x = \frac{3\sigma}{L^3}\left(\frac{Lx^2}{2} - \frac{x^3}{6}\right), \quad (29)$$

where σ is the rms displacement at the tip.

In the case of a single-walled nanotube, because there is only one graphene layer, experimentally we measure only the nanotube width W. This raises the issue of how to select suitable values for a and b. Plausibly, we could assign $a - b = G$, where G is the graphite interlayer spacing of 0.34 nm, and $a = W/2 + \gamma G$ and $b = W/2 - \gamma G$. γ allows for the asymmetry in the electron density of the graphene π bonds on either side of the curved tube, but is expected to be close to $\gamma = 1/2$.[8]

Assuming $\gamma = 0.5$, Eq. (28) can be rewritten in terms of the single-walled tube diameter W as

$$\sigma^2 = 0.8486\frac{L^3 kT}{YWG(W^2+G^2)}. \quad (30)$$

III. EXPERIMENT

Nanotubes prepared by the laser evaporation method[9–11] were dispersed in 99.9% purity ethanol using a probe ultrasonicator. A 300 mesh holey carbon grid was dipped into the suspension and allowed to dry in air. By this method, we were usually able to find isolated single-walled nanotubes which had one free end extended over a hole in the carbon support.

The samples were observed in a Hitachi H9000 NAR TEM operated at 100 kV. The lower accelerating voltage was used to increase contrast and reduce beam damage. Bright field images were collected using a Gatan model 690 slow-scan CCD camera and Digital Micrograph v2.5 software. Samples were surveyed at a magnification of $\times 180\,000$ using an electron dose of ~ 800 electrons $\mathrm{sec}^{-1}\,\mathrm{nm}^{-2}$. All measurements were done at room temperature. The microscope magnification was calibrated by imaging graphite lattice fringes at the eucentric specimen position, and assuming that the spacing was 0.340 nm. The actual magnification is found to be sensitive to the objective lens current. Consequently, during experiments, coarse image focusing was accomplished by raising and lowering the specimen, and fine focusing by adjusting the objective lens current. Efforts were made to maintain the objective lens current within one part in 10^4 of the calibration current in order to minimize errors in the calibration. We estimate that the absolute image magnification is accurate to better than $\pm 1\%$.

We selected nanotubes that were free of large pieces of debris. It is rare to find isolated single nanotubes without at

least some trace of amorphous carbonaceous material on the exterior surface, so we tolerated some contamination provided at least 90% of the tube length is clean. Long nanotubes (>100 nm) tended to have excessive motion at the tips, and would frequently develop kinks. Such nanotubes were avoided in this study.

Once a satisfactorily clean nanotube was located, it was then ''stress-tested'' by increasing the beam current intensity by a factor of about 10 for a fraction of a second. Insecurely anchored nanotubes would twitch, shift, or even disappear. These were rejected. Bright-field images of nanotubes that did not visibly flinch under these conditions were recorded on the slow-scan camera. Typically, nanotubes with free ends in the length range 7–50 nm passed this stress test. In this length range, the entire nanotube free end could be captured on one image frame. Note that in every case the full length of the nanotube is much longer than the projecting end segment that we measure. It is assumed that the end projecting over the hole is anchored by some observable specimen feature.

The exposure time on the CCD was selected so as to acquire at least 500 counts per pixel in the hole area. Frequently, a second or third image of the same nanotube would be recorded to check for any undesirable variations in the image with time, such as drift or a tilting of the nanotube. We did not observe any degradation of the nanotubes under the beam for the total doses used to record data, which were typically $\leqslant 20\,000$ electron nm^{-2} at 100 kV.

In almost all instances, the base of the nanotube under observation, near the presumed anchoring point, could be brought into reasonably sharp focus. The tip, however, was always slightly blurred and could not be brought into sharp focus. Occasionally, the nanotube base would also be blurred, indicating that the nanotube is not securely anchored near this point. Such images were rejected.

Once all the image data had been collected, nanotube lengths and vibration amplitudes were estimated by two methods. In method 1, images were blurred by applying a Gaussian convolution perpendicular to the nanotube axis using Digital Micrograph macros. The blurred image of the base was compared visually with the unblurred image of the tip. The Gaussian standard deviation that produced the best visual match gives an estimate of the tip vibration amplitude, σ. Nanotube dimensions were estimated by direct measurement of the digital images. The nanotube length is estimated by measuring the distance from the tip to the presumed anchoring point, a step that requires some subjective judgment.

To help avert any systematic subconscious bias, the measurements were made ''blind,'' in the sense that the corresponding values for Young's modulus were computed *after* all the measurements were committed. Furthermore, estimates were made independently by two of us (A.K. and M.M.J.T.) to help reduce systematic biases.

In method 2, independent estimates of the nanotube length and tip vibration amplitude were obtained from images of the cleanest nanotubes by a least-squares minimization procedure. First the digital micrographs were expanded by a factor of 4 and rotated by bilinear interpolation, so that the nanotube images were precisely horizontal. The realigned images were then reduced back to their original size. The image expansion step helps minimize information loss incurred in the rotation step.

The nanotube images have now been aligned so that the length is parallel to x. The image can now be considered to comprise a series of intensity line traces $I_x(y)$ along y, perpendicular to x. In the absence of vibration and shot noise, for a perfectly horizontal nanotube, the line traces would be constant, regardless of x. In practice, the traces will differ because of shot noise which depends on the statistics of the illuminating electron beam. Further, since the nanotubes are vibrating, we would expect the line trace near the tip to be a blurred version of the trace near the anchoring point. Given the tip vibration amplitude σ and the nanotube length L, the change in vibration amplitude as a function of position x is known from the equations given in Sec. II. To a very good approximation, the vibration amplitude $u(x)$ varies according to the form given in Eq. (29). Thus, if we know the function $I_0(y)$, the profile $I_x(y)$ of the whole nanotube can be computed by convoluting $I_0(y)$ with a Gaussian

$$I_x(y)=\frac{1}{\sqrt{2\pi}u_x}\int I_0(y'-y)\exp(-y'^2/2u_x^2)dy'. \quad (31)$$

The nanotube length L and tip vibration amplitude σ are treated as unknown. In each image, we select a section of length L_{image} that is clean of any debris or support material. We assume that there is a missing length L_0 to the anchor point. Furthermore, since the nanotube tip usually has a different structure to the shaft, we exclude a length L_{tip} from the analysis. Thus, the true length L is

$$L=L_0+L_{\mathrm{image}}+L_{\mathrm{tip}}, \quad (32)$$

where L_0 is unknown.

A least-squares fit to the image data was then carried out for the region $L_0 \leqslant x \leqslant L_0+L_{\mathrm{image}}$, by making initial guesses for L_0, σ, and the form of $I_0(y)$. A good starting guess for $I_0(y)$ is found by taking the average of the traces $I_x(y)$. Using Powell's quadratically convergent minimization procedure,[12] the optimum form of $I_0(y)$ is found by first generating the image corresponding to the parameters L_0, σ, and $I_0(y)$ using Eqs. (31) and (32). The computed image is subtracted from the data image that we are trying to match, and the sum of the squares of the result is computed. Powell's algorithm computes an optimized profile $I_0(y)$ that minimizes this squared residual for a given L_0 and σ. This process is then repeated for a grid of (L_0,σ) values. The pair of values (L_0,σ) that yields the smallest residual is used to compute Young's modulus.

An attraction of this least-squares method is that no detailed knowledge of the nanotube structure, microscope defocus, spherical aberration, astigmatism, or linear specimen drift is required, since these factors affect all image points equally. The only important assumption is that the nanotube is uniform along its length. Thus, this method works best on the straightest, cleanest nanotube images.

IV. RESULTS AND DISCUSSION

Figure 1 shows three TEM bright field images of single-walled nanotubes protruding over the edge of a hole in a holey carbon support film. The images have been rotated so

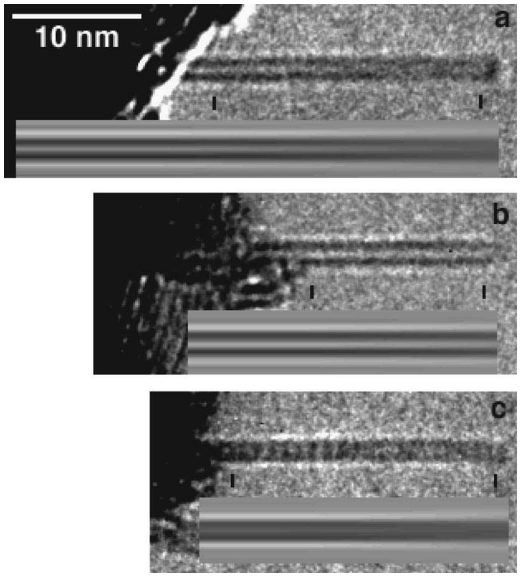

FIG. 1. TEM bright field micrographs of vibrating single-walled nanotubes. Inserted with each micrograph is the simulated image corresponding to the best least-squares fit after adjusting for nanotube free length L and tip vibration amplitude σ using measurement method 2. The tick marks on each micrograph indicate the section of the nanotube shank that was fitted. The nanotube parameters, including nanotube diameter W, with corresponding estimate of Young's modulus Y, are (a) $L=36.8$ nm, $\sigma=0.33$ nm, $W=1.50$ nm, $Y=1.33\pm0.2$ TPa; (b) $L=24.3$ nm, $\sigma=0.18$ nm, $W=1.52$ nm, $Y=1.20\pm0.2$ TPa; and (c) $L=23.4$ nm, $\sigma=0.30$ nm, $W=1.12$ nm, $Y=1.02\pm0.3$ TPa.

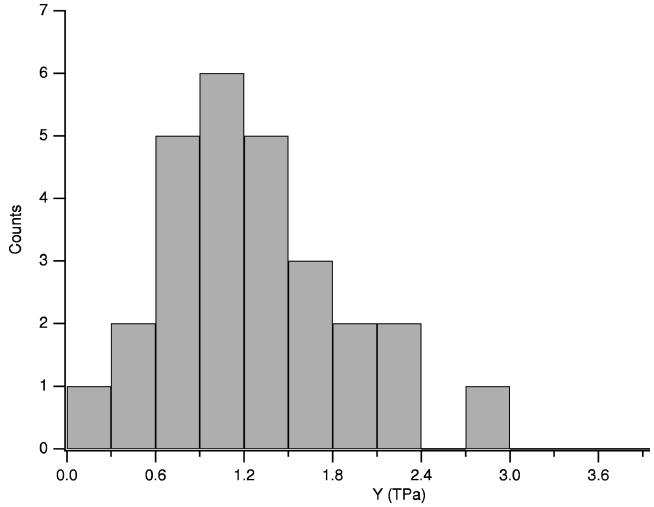

FIG. 2. Histogram of Young's modulus values Y obtained from 27 nanotubes. The nanotube lengths L and tip vibration amplitudes σ were estimated directly from the digital micrographs using method 1, as described in the text. The mean value is $\langle Y\rangle=1.3-0.4/+0.6$ TPa.

that the nanotubes are anchored at the left, and the free vibrating tips are to the right. The simulated full-length images corresponding to the best fit according to our least-squares optimization (method 2) are shown inset in each image. The best fits correspond to Young's moduli of 1.33 ± 0.2, 1.20 ± 0.2, and 1.02 ± 0.3 TPa, respectively. When we independently estimated the length and vibration amplitude by eye, using method 1, the values 1.22, 1.3, and 0.69 TPa were obtained for these three nanotubes. This is in good agreement with the values obtained by the least-squares optimization.

The length and vibration amplitudes of a further 24 nanotubes were estimated by method 1. The nanotube diameters were in the range 1.0–1.5 nm. These nanotubes were insufficiently pristine to be reliably optimized by method 2. Most of these latter sets of nanotubes had slight visible contamination. Such contaminating particles will affect the vibration frequency by raising the moment of inertia, but will have an insignificant affect on the vibration amplitude since they do not form an extended coating. Figure 2 is a histogram showing the spread in the estimated Y values for the 27 nanotubes. The mean value is $\langle Y\rangle=1.3-0.4/+0.6$ TPa, and the median value is a little lower, 1.1 TPa. This mean value is consistent with the three values obtained by method 2. The distribution is not symmetrical about the mean, displaying a tail extending to the higher values. To understand the significance of this spread, and the reliability of the mean value, $\langle Y\rangle$, it is important to discuss the experimental errors in more detail.

An important experimental parameter is the image magnification. The equation for Y [Eq. (28)] depends on length measurements as $a^4\sigma^2/L^3$, which therefore depends on magnification M as M^{-3}. Systematic errors in M introduce relative errors in Y as $\Delta Y/Y=3\Delta M/M$. We estimate that our magnification calibration is accurate to within 1%, which contributes a 3% error in Y.

The length of each tube, L, was estimated by measuring the projected length from the tip to the perceived anchor point, the latter usually being the entry point into a thick clump of carbonaceous material near the edge of the hole. Not all nanotubes are expected to be perfectly horizontal, thus our length measurements, L', will tend to be underestimated according to $L'=L\cos\theta$ for a nanotube at an angle θ to the horizontal. It is quite plausible that the nanotubes we measured had an angular spread of up to about $\pm30°$ to the horizontal, giving rise to a spread in L'^3 of $(0.65–1.0)\times L^3$. Thus, from projection errors alone, we may be systematically underestimating L^3 by an average of about 20%. A further source of error in L arises when the true anchor point lies deeper within the carbonaceous clump than the perceived point of entry. By comparing the three L values that were obtained by both methods 1 and 2, we estimate the error in locating the anchor point to be around $\Delta L/L\approx10\%$.

The depth of focus ΔF was estimated by simulating a focal series for a typical 1.4-nm-diam nanotube using the MACTEMPAS multislice program,[13] and was found to be approximately $\Delta F=\pm10$ nm. This is larger than the uncertainty in the tip elevation relative to the base, which is ±7 nm for an $L=50$ nm tilted at 30°. It is therefore reasonable to ignore the contribution to the tip blurring of focal gradients along a tilted nanotube.

The standard deviation of the tip motion, σ, was typically in the range 1–3 nm. However, the typical image contrast across a single-walled carbon nanotube of diameter 1.41 nm is about 3%. In a typical image with around 1000 counts per pixel, the shot noise is also at the 3% level. Because of the low signal-to-noise, and the subjective nature of measurements made by method 1, two of us (A.K. and M.M.J.T.) independently assessed the standard deviation, and the re-

sults were found to be consistent with each other to within $\pm 20\%$. Because of the σ^2 dependence, this contributes an error of approximately $\pm 40\%$ in Y.

The nanotube width W was estimated by taking the average of several measurements near the base. Nanotubes were consistently uniform along their length. The image features to measure, in order to obtain accurate physical diameters, were determined by simulating images of nanotubes by using the MACTEMPAS[13] multislice program. The measured accuracy of W for each nanotube is conservatively estimated to be about $\pm 5\%$, contributing an error of $\pm 15\%$ in Y [see Eq. (30)].

Nanotubes were assumed to be at room temperature, 14–16 °C, as measured by a thermocouple near the sample. From previous experiments,[6] it is known that the electron beam contributes a small amount of heating which is dependent on the beam intensity. This is estimated to be around 20–40 °C. This correction will tend to increase the average value of Y. No adjustment was made for this temperature correction in the data of Fig. 2.

It is assumed in this analysis that the extraneous carbonaceous material that frequently litters the nanotubes has a negligible impact on the stiffness. It is expected that the additional mass will decrease the resonant vibration frequency of the nanotubes, but not the vibration amplitude. However, we need to be mindful that extraneous particles may tend to deform nanotube walls locally, which may in turn lower the stiffness because of an enhanced tendency to buckle. For this reason, bent and heavily contaminated nanotubes were avoided.

It is clear from the above discussion that the expected accuracy of Y for any individual nanotube, as estimated by method 1, will be no better than about $\pm 60\%$. However, when averaged over a large number of nanotubes, the average value will be less susceptible to random measurement errors. We have identified two systematic errors, namely the length estimate and the temperature estimate. We have argued that the length is systematically underestimated such that, on average, the measured quantity L^3 is only 80% of the true value. Furthermore, the actual temperature is about 10% ($\sim$30 K) higher than the nominal value of 300 K. Thus the ratio L^3T may be systematically underestimated by a factor of about 25%. The data of Fig. 2 have not been corrected to compensate for this factor.

From methods 1 and 2, we get a weighted average value of $\langle Y \rangle = 1.25$ TPa. It is clear that we are inferring values for the bending modulus that appear to be systematically higher than the in-plane elastic modulus $1/S_{11}$ reported for graphite. However, we should bear in mind that we are comparing the strongly curved, seamless, graphene sheet of the nanotube with bulk planar graphite. Furthermore, we are assuming that we can assign an inner and outer radius to a single-walled nanotube based on the graphite interlayer spacing. Given the strong $(a^4 - b^4)$ dependence of Y on the inner and outer radii b and a, respectively, small adjustments to b and a can have a potentially large affect on the derived value of Y.

The accepted values for graphite have a large spread, depending on the sample and the measurement process. Vibration studies done on as-is and neutron-irradiated single-crystal graphite[14] yielded a mean value for G ($=1/S_{44}$, shear modulus parallel to the basal planes) of 0.1 GPa. On neutron irradiation (flux: 4×10^{19} neutrons/cm^2), it is believed that the modulus is dominated by E ($=1/S_{11}$, Young's modulus parallel to the basal planes), and the value is quoted as 360 ± 60 GPa. However, measurements on samples with a length to thickness ratio $l/t > 50$ yielded higher values for E and the true value is given as 600 ± 200 GPa. Other workers report resonant bar tests that yield an average value of 895 GPa for $1/S_{11}$ before neutron irradiation and 940 GPa after irradiation. Static tests give 878 GPa and 912 GPa before and after irradiation for $1/S_{11}$.[15] Measurements on vapor-grown carbon fibers using a vibrating-reed technique gave an average value of 695 GPa with a maximum value of 1017 GPa.[16] It is worth noting that the oft-quoted 1.02 TPa value for the modulus of graphite is actually obtained from measurements on compression-annealed pyrolytic graphite (CAPG).[5] In these samples, the c axes are all parallel to each other but the a axes are arbitrarily rotated with respect to each other and the sample is not a true single crystal of graphite. Resonant bar tests on CAPG yielded an average $1/S_{11}$ of 943 GPa. Static tests gave a similar value of 920 ± 120 GPa. The maximum value of the in-plane $1/S_{11}$ is 1.02 ± 0.03 TPa and the in-plane shear modulus ($1/S_{44}$) ranged from 0.18 to 0.31 GPa. Clearly, the true value of the in-plane modulus of graphite is not known with certainty. The values of the other elastic constants for graphite are summarized elsewhere,[5] and they also show a significant spread in values. Theoretical calculations give a value for the in-plane modulus of a 1-nm-diam tube ranging from 0.5 TPa (Ref. 17) to about 5.5 TPa.[4,2] Also, different trends have been predicted for the dependence of Young's modulus on the radius of the tube.[18,17,3] However, significant changes are only predicted for tubes much smaller than those in our samples. Together with the narrow range of diameters in our sample and uncertainty in the individual measurements, it is not surprising that we cannot confirm any of these trends. Measurements on multiwalled nanotubes[6] using a technique similar to that described here yielded an average value for Young's modulus of 1.8 TPa, with an order of magnitude spread between individual nanotubes. This spread is probably due in part to the presence of structural imperfections in the nanotubes, such as the nesting of cylinders which can create a joint or "knuckle" thereby weakening the tube, and in part to experimental uncertainties, such as the estimation of the free-standing length and the tip vibration amplitude. Given the experimental uncertainties in this work, and in the previous work on multiwalled nanotubes,[6] no firm conclusions can be made about the relative average stiffness of single-walled nanotubes versus multiwalled nanotubes. However, there are persistent indications that both have a higher Young's modulus than graphite.

The observation of consistently higher values for Young's modulus of nanotubes as compared with bulk graphite can mean one of two things. Either the particular cylindrical structure of the graphene sheet results in increased strength, or the accepted value for graphite is underestimated. The latter is a serious possibility considering the nature of the samples used in the measurement. Further studies are necessary to resolve this issue.

ACKNOWLEDGMENT

The authors wish to thank M. E. Bisher for valuable assistance.

[1] M. S. Dresselhaus, G. Dresselhaus, K. Sugihara, I. L. Spain, and H. A. Goldberg, *Graphite Fibers and Filaments* (Springer-Verlag, New York, 1988).
[2] G. Overney, W. Zhong, and D. Tomanek, Z. Phys. D **27**, 93 (1993).
[3] D. H. Robertson, D. W. Brenner, and J. W. Mintmire, Phys. Rev. B **45**, 12 592 (1992).
[4] B. I. Yakobson, C. J. Brabec, and J. Bernholc, Phys. Rev. Lett. **76**, 2511 (1996).
[5] O. L. Blakslee, D. G. Proctor, E. J. Selden, G. B. Spence, and T. Weng, J. Appl. Phys. **41**, 8 (1970).
[6] M. M. J. Treacy, T. W. Ebbesen, and J. M. Gibson, Nature (London) **381**, 678 (1996).
[7] E. W. Wong, P. E. Sheehan, and C. M. Lieber, Science **277**, 1971 (1977).
[8] J. C. Charlier, Ph. Lambin, and T. W. Ebbesen. Phys. Rev. B **54**, 8377 (1996).
[9] E. Dujardin, T. W. Ebbesen, A. Krishnan, and M. M. J. Treacy, Adv. Mater. **10**, 611 (1998).
[10] T. Guo, P. Nikolaev, A. Thess, D. T. Colbert, and R. E. Smalley, Chem. Phys. Lett. **243**, 49 (1995).
[11] A. Thess, R. Lee, P. Nikolaev, H. Dai, P. Petit, J. Robert, C. Xu, Y. H. Lee, S. G. Kim, A. G. Rinzler, D. T. Colbert, G. E. Scuseria, D. Tomanek, J. E. Fisher, and R. E. Smalley, Nature (London) **273**, 483 (1996).
[12] W. H. Press, S. A. Teukolsky, W. T. Vetterling, and B. P. Flannery, *Numerical Recipes in C* (Cambridge University Press, Cambridge, 1992).
[13] R. Kilaas, Ph.D. thesis, Lawrence Berkeley Laboratories, 1988.
[14] C. Baker and A. Kelly, Philos. Mag. **9**, 927 (1964).
[15] E. J. Seldin and C. W. Nezbeda, J. Appl. Phys. **41**, 8 (1970).
[16] R. L. Jacobsen, T. M. Tritt, J. R. Guth, A. C. Ehrlich, and D. J. Gillespie, Carbon **33**, 1217 (1995).
[17] C. F. Cornwell and L. T. Wille, Solid State Commun. **101**, 555 (1997).
[18] J. P. Lu, Phys. Rev. Lett. **79**, 1297 (1997).
[19] E. Hernández, C. Goze, P. Bernier, and A. Rubio, Phys. Rev. Lett. **80**, 4502 (1998).